remote sensing

MDPI

Article

Impacts of Climate Change on European Grassland Phenology: A 20-Year Analysis of MODIS Satellite Data

Edoardo Bellini [1], Marco Moriondo [2,*], Camilla Dibari [1], Luisa Leolini [1], Nicolina Staglianò [1], Laura Stendardi [1], Gianluca Filippa [3], Marta Galvagno [3] and Giovanni Argenti [1]

[1] Department of Agriculture, Food, Environment and Forestry (DAGRI), University of Florence, 50144 Florence, Italy
[2] Institute of BioEconomy, Italian National Research Council (IBE-CNR), 50019 Sesto Fiorentino, Italy
[3] Environmental Protection Agency of Aosta Valley-Climate Change Unit, Saint-Christophe, 11100 Aosta, Italy
* Correspondence: marco.moriondo@cnr.it; Tel.: +39-0552755747

Abstract: The use of very long spatial datasets from satellites has opened up numerous opportunities, including the monitoring of vegetation phenology over the course of time. Considering the importance of grassland systems and the influence of climate change on their phenology, the specific objectives of this study are: (a) to identify a methodology for a reliable estimation of grassland phenological dates from a satellite vegetation index (i.e., kernel normalized difference vegetation index, kNDVI) and (b) to quantify the changes that have occurred over the period 2001–2021 in a representative dataset of European grasslands and assess the extent of climate change impacts. In order to identify the best methodological approach for estimating the start (SOS), peak (POS) and end (EOS) of the growing season from the satellite, we compared dates extracted from the MODIS-kNDVI annual trajectories with different combinations of fitting models (FMs) and extraction methods (EM), with those extracted from the gross primary productivity (GPP) measured from eddy covariance flux towers in specific grasslands. SOS and POS were effectively identified with various FM×EM approaches, whereas satellite-EOS did not obtain sufficiently reliable estimates and was excluded from the trend analysis. The methodological indications (i.e., FM×EM selection) were then used to calculate the SOS and POS for 31 grassland sites in Europe from MODIS-kNDVI during the period 2001–2021. SOS tended towards an anticipation at the majority of sites (83.9%), with an average advance at significant sites of 0.76 days year^{-1}. For POS, the trend was also towards advancement, although the results are less homogeneous (67.7% of sites with advancement), and with a less marked advance at significant sites (0.56 days year^{-1}). From the analyses carried out, the SOS and POS of several sites were influenced by the winter and spring temperatures, which recorded rises during the period 2001–2021. Contrasting results were recorded for the SOS-POS duration, which did not show a clear trend towards lengthening or shortening. Considering latitude and altitude, the results highlighted that the greatest changes in terms of SOS and POS anticipation were recorded for sites at higher latitudes and lower altitudes.

Keywords: start of season (SOS); peak of season (POS); end of season (EOS); vegetation index; GPP; kNDVI

Citation: Bellini, E.; Moriondo, M.; Dibari, C.; Leolini, L.; Staglianò, N.; Stendardi, L.; Filippa, G.; Galvagno, M.; Argenti, G. Impacts of Climate Change on European Grassland Phenology: A 20-Year Analysis of MODIS Satellite Data. *Remote Sens.* **2023**, *15*, 218. https://doi.org/10.3390/rs15010218

Academic Editors: Jungho Im, Seonyoung Park and Cheolhee Yoo

Received: 18 November 2022
Revised: 26 December 2022
Accepted: 27 December 2022
Published: 30 December 2022

1. Introduction

Phenology is defined as the "study of the timing of recurring biological events, the causes of their timing with regard to biotic and abiotic forces, and the interrelation among phases of the same or different species" [1]. Vegetation phenology specifically addresses processes linked to the plant cycle, such as leaf emergence, flowering, leaf colouration and fall [2]. These are controlled by molecular mechanisms inside the organism and driven by factors such as temperature and photoperiod [3].

The study of plant phenology through on-field observations, although a reliable approach [4], is time-consuming and costly when applied at large spatial scales or over

long time series. Moreover, observed phenological data are site specific, often sparsely distributed and measured for a few plant species only and at discrete phenophases [5].

To overcome these issues, the collection of data and information on phenology through remote sensing devices and methodologies has become of great importance over the years as a result of scientific advances in this field of study. Within remote sensing, different types of technologies can be considered for phenological analysis, such as satellites equipped with specific sensors [6–8] or Phenocam digital cameras [9–12]. Taking into account satellite images and the different vegetation indices derived from them [13], the use of these data has been widely experimented in the literature in different environments, such as evergreen forests, deciduous forests, croplands and grasslands [14,15], to assess the vegetation cycles through the extraction of phenological dates of the start, peak or end of the growing season. Approaches to retrieving these relevant phenological dates from vegetation indices have been previously investigated with regard to the smoothing and filtering functions of raw satellite data [16] and date extraction techniques [15]. Furthermore, there has been the development of specific software, such as Phenopix [17], that simplified and automated data processing techniques for phenological studies.

In addition to data collected from on-field and remote sensing observations, another important source of information for studying phenology is the gross primary productivity (GPP), i.e., the total amount of CO_2 fixed by plants through vegetation photosynthesis [18–20], elaborated from eddy covariance measurements at flux tower sites. Since phenology is one of the most important controls of the interannual variability of GPP [21,22], these measurements have been used in a number of studies as a proxy for vegetation phenology [15,23]. Unlike phenological on-field observations that are based on the human eye, GPP is focused on photosynthetic phenology, which is a result of both plant canopy development and light use efficiency [24]. By measuring the photosynthetic carbon uptake of the vegetation canopy, dates of start and end of season elaborated from GPP measurements provide indications of when ecosystems switch from a source to a sink of C, and vice versa [25]. Given the importance of these data, GPP measurements are also used to evaluate the efficiency of remote sensing data in estimating ecosystem phenological dates [26,27].

In the last decades, the study of phenological events in plant communities has become increasingly important to assess the impacts of climate warming on vegetation cycles, with consequences on agricultural, forest and grassland systems [28,29]. With a specific focus on the latter, monitoring grassland ecosystems, which cover ca. 70% of the total world agricultural area [30], has gained interest due to the large amount of ecosystem services they provide, e.g., erosion protection, water regulation, carbon storage, biodiversity, food for animal production systems and wildlife, aesthetic and recreational functions [31–34]. Given the huge spatial extent of these environments and the large number of functions they perform, understanding trends and potential climate-induced shifts in grassland phenology is impelling [35]. Studies of different environments in Europe have already shown changes in phenological phases over the period 1951–2018 in a limited number of countries for which long series of observed data were available [36].

In this regard, long time series of vegetation indices, such as those elaborated from MODIS satellite images, allow the study of phenology over a relatively long period of time, providing information at 250 m spatial resolution and 16-day temporal resolution. This involves assessing changes in phenological dates over the past decades and quantifying the extent of the impacts of climate change on the plant life cycle that are already visible in grassland systems [37]. Analyses of satellite-derived phenology over the period 1982–2001 also showed a general advance driven by climate change [38]. However, a comprehensive phenological analysis specific to European grasslands in recent decades is still lacking, as is the evaluation of the impact of rising temperatures on these changes.

Building on these premises, the objectives of this research were, therefore, twofold:

(*i*) Identification of a reliable approach to determine the start (SOS), peak (POS) and end of the growing season (EOS) through the use of specific vegetation indices (i.e., kernel

normalized difference vegetation index, kNDVI) processed from MODIS satellite imagery, relying on observed GPP data from grassland sites as comparison;

(*ii*) Analysis of phenological trends of different European grasslands in the period 2001–2021 using the methodology identified in point (*i*) in order to highlight possible changes in the dates of SOS, POS and EOS and the relevant climatic drivers.

2. Materials and Methods

2.1. Preliminary Analysis and Optimisation of the Extraction Method

In order to analyse the trend of phenological dates of a representative dataset of European grasslands over the last 20 years, it was necessary to identify the best strategy for extracting key grassland phenological phases (i.e., SOS, POS and EOS) from satellite images (Figure 1). The effectiveness of the use of satellite-derived vegetation indices (i.e., kNDVI) in the assessment of grassland phenological stages was evaluated using as a benchmark observed seasonal trend of grasslands' gross primary production (GPP) as fitted by different models (FM) and extraction methods (EM). The complete procedure is given below.

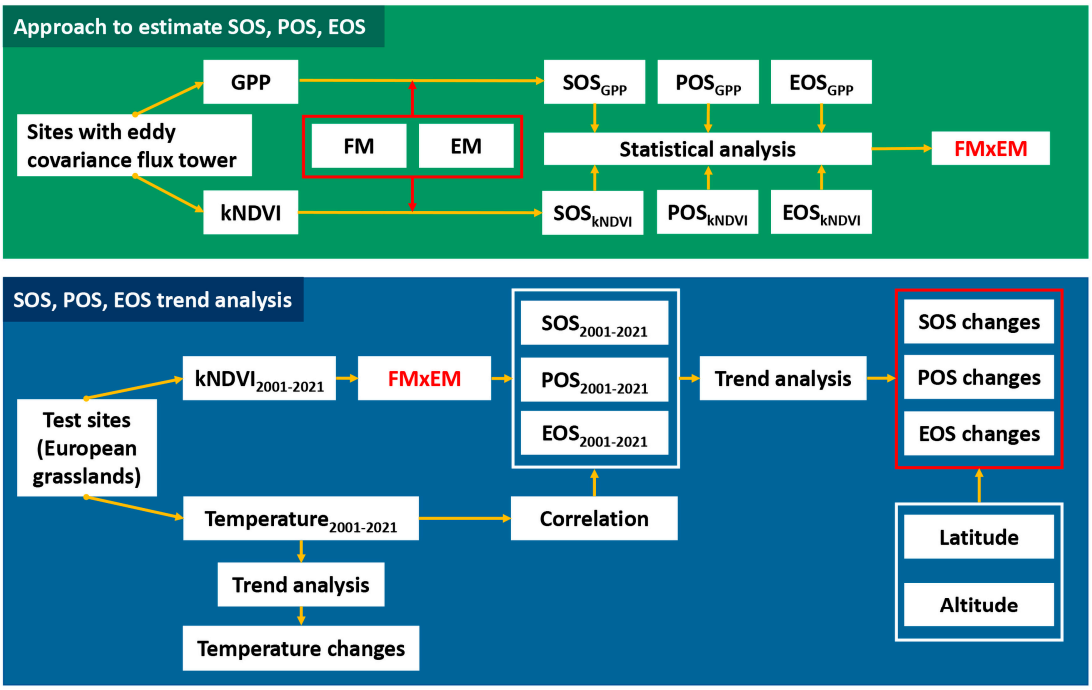

Figure 1. Workflow of the methodology, divided into "Approach to estimate SOS, POS, EOS" (2.1) and "SOS, POS, EOS trend analysis" (2.2).

2.1.1. GPP Data and Study Areas

Daily GPP data (g C m^{-2} d^{-1}), used as observed values of grassland growing seasons, were collected at study sites of the FLUXNET (https://fluxnet.org/, accessed on 5 July 2022 [39]) and European Fluxes Database Cluster (http://www.europe-fluxdata.eu/, accessed on 7 July 2022) networks. At these sites, CO_2 flux of grasslands is regularly measured from in situ towers by means of the eddy covariance method, and then further partitioned into ecosystem respiration and GPP [40]. From these two networks, 9 study areas in Europe with different altitudinal and botanical conditions were selected in order to obtain a representative European dataset. The list of study areas with the relative information is reported in Table 1. From the GPP patterns elaborated from this dataset, SOS, POS and EOS were extracted with the different approaches that are explained in Section 2.1.3.

Table 1. List of grassland sites used to obtain daily GPP data. Mamsl represents meters above mean sea level (m), while EFDC represents the European Fluxes Database Cluster.

ID	Site	Country	Network	Lat	Lon	Mamsl	Years
AT-Neu	Neustift [41]	Austria	FLUXNET	47.1167	11.3175	970	2002–2012
CH-Cha	Chamau [42]	Switzerland	FLUXNET	47.2102	8.4104	393	2002–2008
CH-Fru	Früebüel [43]	Switzerland	FLUXNET	47.1158	8.5378	982	2005–2014
CZ-BK2	Bily Kriz	Czech Republic	FLUXNET	49.4944	18.5429	855	2006–2012
DE-Gri	Grillenburg [44]	Germany	FLUXNET	50.9500	13.5126	385	2004–2018
DE-Rur	Rollesbroich [45]	Germany	FLUXNET	50.6219	6.3041	514	2011–2018
IT-Mal	Malga Arpaco	Italy	EFDC	46.1140	11.70334	1662	2003–2004
IT-Mbo	Monte Bondone [46]	Italy	FLUXNET	46.0147	11.0458	1550	2004–2013
IT-Tor	Torgnon [25]	Italy	FLUXNET	45.8444	7.5781	2160	2009–2018

2.1.2. Satellite Data

For the purpose of the study, we selected the Moderate Resolution Imaging Spectroradiometer (MODIS) imagery to retrieve the vegetation index from which to extract SOS, POS and EOS, corresponding to what was assessed for GPP data. Despite its lower spatial resolution compared to other more recent satellites (e.g., Sentinel-2), MODIS provides a long-time series of data allowing the analysis of phenological trends in European grasslands over the last decades.

The vegetation index used to reproduce the growing season of grasslands was the kernel NDVI (kNDVI), a specific vegetation index used to reconstruct GPP patterns in different environments, including grasslands [47]. The kNDVI is calculated as follows:

$$\text{kNDVI} = \frac{1 - k(n,r)}{1 + k(n,r)} \quad (1)$$

where n and r refer to the reflectance in the near-infrared (NIR) and red bands (RED), respectively, BAND 2 and BAND 1 in MODIS at 250 m spatial resolution and 8 days of temporal resolution (product: MODIS/006/MOD09Q1), while the kernel function k measures the similarity between these two bands. We used the RBF kernel proposed by the same authors [47]:

$$k(a,b) = exp\ \frac{\left(-(a-b)^2\right)}{((2\sigma)^2)} \quad (2)$$

where the σ parameter controls the notion of the distance between the NIR and RED bands, elaborated as the mean distance between these two bands:

$$\sigma = 0.5(n + r) \quad (3)$$

For each site, kNDVI values were then processed from the MODIS RED and NIR bands according to the previous formulas, using the specific coordinates of the grassland sites with eddy covariance stations.

2.1.3. Fitting Models and Extraction Methods

In order to perform an accurate satellite analysis of phenological date trends over the period 2001–2021, different fitting models (FMs) and date extraction methods (EMs) were applied both to raw data of GPP and kNDVI to find the most performing FM×EM approach. The methodology was then chosen taking into account the results of the comparison between SOS, POS and EOS extracted from GPP and kNDVI annual patterns.

Consequently, raw data of GPP and kNDVI underwent a process for retrieving the phenological dates of SOS, POS and EOS. Specifically, using a work package for phenological analysis within the R work environment (*phenopix*, [17]), the annual patterns of GPP and kNDVI were subjected to the fitting operation and, subsequently, to SOS, POS and EOS extraction.

The FM used in this comparison were 4: Elmore et al. [48] (ELM), Gu et al. [49] (GU), Beck et al. [50] (BEC) and Klosterman et al. [51] (KLS). These methods fitted different double logistic curves to the raw data of GPP and kNDVI according to the aforementioned studies. Equations of ELM, GU, BEC and KLS [17] are shown below:

$$f(t) = mn + (mx - mn) \cdot \left(\frac{1}{1 + e^{(m'_3 - t)/m'_4}} - \frac{1}{1 + e^{(m'_5 - t)/m'_6}} \right) \quad (4)$$

$$f(t) = y_0 + \frac{a_1}{\left[1 + e^{-(t - t_{01})/b_1}\right] c_1} - \frac{a_2}{\left[1 + e^{-(t - t_{02})/b_2}\right] c_2} \quad (5)$$

$$f(t) = mn + (mx - mn) \cdot \left(\frac{1}{1 + e^{(-rsp \cdot (t - sos))}} + \frac{1}{1 + e^{(-rau \cdot (t - eos))}} \right) \quad (6)$$

$$f(t) = (a_1 t + b_1) + \left(a_2 t^2 + b_2 t + c\right) \cdot \left(\frac{1}{\left[1 + q_1 e^{-h_1 (t - n_1)}\right] v_1} - \frac{1}{\left[1 + q_2 e^{-h_2 (t - n_2)}\right] v_2} \right) \quad (7)$$

The selected FMs optimise a different number of parameters and hence present diverse flexibility in fitting raw data. For a more comprehensive understanding of the methods and curve parameters, see the corresponding publications.

The GPP and kNDVI curves obtained after FM application were then used to extract SOS, POS and EOS with four extraction methods [17]: three working on inflection points of the derivatives (*Klosterman*, *Gu*, *Derivatives*), and one that identifies the dates when a fixed threshold of the seasonal amplitude is reached (*Thresholds*). Specifically, *Klosterman* is based on local extremes in the rate of change of curvature k [52], *Derivatives* on local extremes in the first derivative, and *Gu* on a combination of local maxima in the first derivative [49]. Regarding the *Thresholds* method, in this trial we tested different values for the fixed threshold: 10 ($TRS_{0.1}$), 20 ($TRS_{0.2}$), 30 ($TRS_{0.3}$), 40 ($TRS_{0.4}$) and 50% ($TRS_{0.5}$) of the seasonal amplitude.

2.1.4. Evaluation Criteria

The statistical analysis performed to evaluate the FMxEM methodology that provides the best match between SOS, POS and EOS from observed values (i.e., GPP) and satellite-derived values (i.e., kNDVI) was conducted using four statistical indicators: the coefficient of determination (R^2), the mean absolute error (MAE), Akaike's information criterion (AIC) and root-mean-square error (RMSE).

The four indices are calculated as follows:

$$R^2 = \frac{\sum_{i=1}^{n} \left(y_i - \underline{y}_i\right)^2}{\sum_{i=1}^{n} \left(y_i - \hat{y}_i\right)^2} \quad (8)$$

$$MAE = \frac{\sum_{i=1}^{n} \left|y_i - \hat{y}_i\right|}{n} \quad (9)$$

$$AIC = 2k - 2\ln\ln\left(\hat{L}\right) \quad (10)$$

$$RMSE = \sqrt{\frac{1}{n} \sum_{i}^{n} \left(y_i - \hat{y}_i\right)^2} \quad (11)$$

where n represents the number of observations, y_i the observed value, $\underline{y}_i$ the mean observed value, $\hat{y}_i$ the simulated value, k the number of estimated parameter and $\hat{L}$ the maximum value of the likelihood function. In order to exclude outlier points, FM×EM approaches were evaluated by excluding years in which the difference between observed and simulated phenological dates was higher than 70 days. The percentage of points used out of the total was reported as *pp* (point percentage).

2.2. SOS, POS, EOS Analysis in the 2001–2021 Period

The approach to extract SOS, POS and EOS from MODIS satellite imagery was selected after the comparison between phenological dates extracted from kNDVI and observed GPP and then applied to different grassland systems in Europe over the period 2001–2021. Subsequently, the influence of seasonal mean temperatures was evaluated to understand the impact of climate change (Figure 1).

2.2.1. Study Areas and Meteorological Time Series

The analysis of the period 2001–2021 was performed across different grassland sites in Europe. Study areas were identified from WEkEO (https://www.wekeo.eu/services accessed on 27 July 2022), the EU Copernicus DIAS reference service for environmental data, virtual processing environments and skilled user support. From the specific layer that identifies the category "grasslands", we selected 31 different sites (Figure 2) from which the MODIS-kNDVI annual patterns to retrieve SOS, POS and EOS were elaborated and extracted. Sites were selected to include areas with different altitudinal and latitudinal conditions to increase the representativeness of the dataset (Table 2).

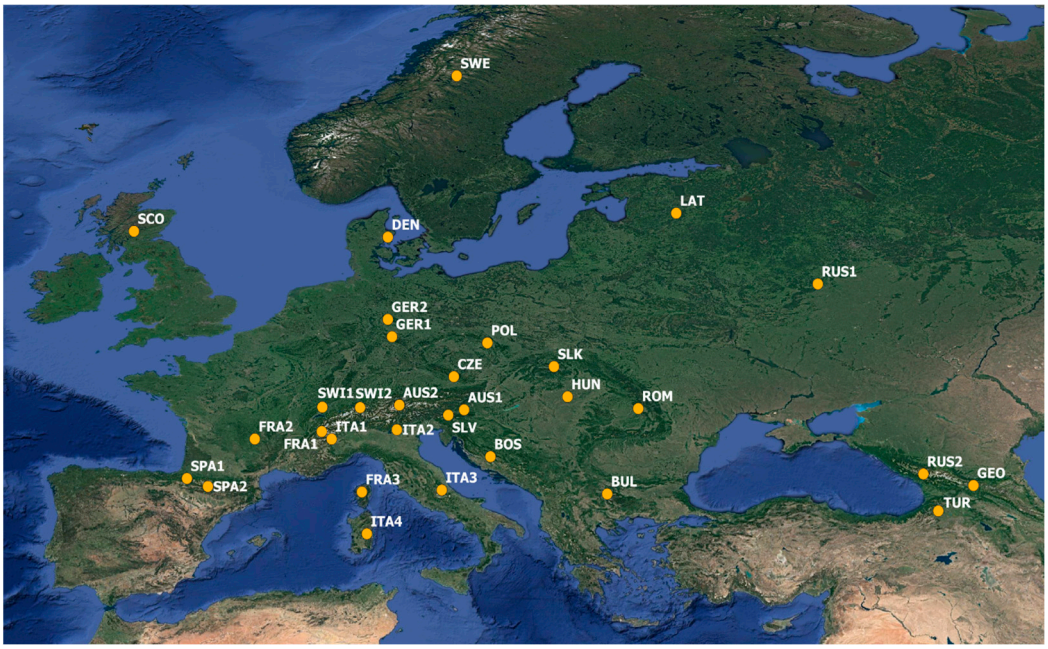

Figure 2. Distribution of study areas across Europe.

Table 2. European grassland sites selected for phenological analysis during the period 2001–2021.

Site ID	Country	Latitude	Longitude	Altitude	Meteo Station	Meteo Years
AUS1	Austria	46.7782°N	14.9746°E	1740	Feistritz Ob Bleiburg	2008–2021
AUS2	Austria	47.0373°N	11.2085°E	1931	Obergurgl	2002–2021
BOS	Bosnia	44.2219°N	16.5075°E	1092	Livno	2001–2021
BUL	Bulgaria	42.1875°N	23.2977°E	2434	Mussala Top Sommet	2001–2021
CZE	Czech Republic	48.5850°N	14.3765°E	642	Budejovice Roznov	2001–2021
DEN	Denmark	56.1995°N	10.5378°E	40	Aarhus	2001–2021
FRA1	France	45.5949°N	6.6931°E	1812	Bourg St Maurice	2001–2021
FRA2	France	45.1842°N	2.7997°E	1169	Aurillac	2001–2021
FRA3	France	42.2984°N	9.0294°E	1125	Ile Rousse	2001–2021
GEO	Georgia	42.6512°N	44.601°E	2258	Pasanauri	2004–2016

Table 2. *Cont.*

Site ID	Country	Latitude	Longitude	Altitude	Meteo Station	Meteo Years
GER1	Germany	50.7660°N	10.7831°E	518	Erfurt	2005–2021
GER2	Germany	51.7090°N	10.5377°E	697	Fritzlar	2001–2021
HUN	Hungary	47.4892°N	20.9926°E	276	Debrecen	2001–2021
ITA1	Italy	45.1806°N	7.2695°E	1975	Bousson	2006–2021
ITA2	Italy	45.6908°N	11.0631°E	1576	Paganella Mountain	2001–2021
ITA3	Italy	42.4005°N	13.6756°E	1623	No station	
ITA4	Italy	40.0129°N	9.3181°E	1464	Perdasdefogu	2006–2021
LAT	Latvia	57.5046°N	27.3139°E	581	Aluksne	2004–2020
POL	Poland	50.4299°N	16.3272°E	630	Klodzko	2001–2021
ROM	Romania	46.8456°N	25.1027°E	1192	Batos	2014–2021
RUS1	Russia	53.6425°N	35.5488°E	165	Bryansk	2001–2021
RUS2	Russia	43.2756°N	41.6877°E	2544	Teberda	2013–2020
SCO	Scotland	56.5194°N	4.2276°W	559	Glen Ogle	2001–2021
SLK	Slovakia	49.1370°N	20.2007°E	1357	No station	
SLV	Slovenia	46.4887°N	14.0553°E	1238	Ratece	2013–2021
SPA1	Spain	43.0329°N	1.147°W	992	Pamplona	2001–2021
SPA2	Spain	42.5973°N	0.0713°E	1759	No station	
SWE	Sweden	64.9977°N	14.5455°E	854	Stekenjokk	2002–2021
SWI1	Switzerland	46.9242°N	6.7304°E	1219	Bullet La Fretaz	2002–2021
SWI2	Switzerland	46.9014°N	8.9249°E	1749	Disentis Sedrun	2001–2021
TUR	Turkey	41.2610°N	42.5550°E	2524	Ardahan	2009–2021

Coordinates were reported in WGS84.

Meteorological data were extracted from the National Centers for Environmental Information (NCEI) stations of the National Oceanic and Atmospheric Administration (NOAA) dataset (https://www.ncei.noaa.gov/maps/daily/ accessed on 29 July 2022). Wherever possible, mean daily temperatures were collected from stations located in the closest proximity to the grassland site coordinates.

2.2.2. Procedure and Trend Analysis

In order to proceed with the extraction of phenological dates (i.e., SOS, POS and EOS), an area of 250 × 250 m cleared of any interference (bare soil, rocks, shrubs, trees) was identified within each grassland site on the WEkEO portal. From the centroid of this area, coordinates were subsequently extracted and used to identify the MODIS pixel for the processing of the kNDVI vegetation index. For each pixel, annual patterns of kNDVI for the period 2001–2021 were then recreated. From these trends, dates of SOS, POS and EOS were extracted according to the results obtained by the different approaches tested during the preliminary analysis. Specifically, the choice of methods took into account the need to use a single fitting model in order to extract SOS, POS and EOS from the same curve. Instead, the extraction methods were selected in accordance with the best results obtained in the preliminary analysis for each phenological date (i.e., SOS, POS and EOS) in order to achieve better accuracy. The selected FM×EM approaches (same FM, different EM for phenological date) were then applied to all sites and years to estimate SOS, POS and EOS.

For each site, values of SOS, POS and EOS depicting a difference with the mean value higher than twice the value of deviance were discarded so as to exclude outliers from the analysis. Furthermore, in order to smooth out short-term fluctuations, a moving

average with a three-year window was applied on phenological dates during the time period considered.

After extracting and filtering SOS, POS and EOS, advances or delays in the cycle of grassland vegetation during the time period considered (2001–2021) were analysed.

The results were then correlated with the processed weather data extracted from stations located in proximity to the study areas. Specifically, daily data of temperatures at each site were aggregated seasonally: winter (January, February and March), spring (April, May and June), summer (July, August and September) and autumn (October, November and December). Then, as well as for phenological dates, a moving average with a three-year window was performed on average seasonal values of mean temperature to smooth fluctuations and highlight temporal trends. Data were elaborated with a linear regression analysis in order to evaluate possible changes in mean seasonal temperatures over the period 2001–2021.

Finally, mean temperature data were compared through a correlation analysis to phenological dates extracted from kNDVI patterns to investigate the potential impact of this factor on advances or delays in the grassland growing season. As in [38], analysis of phenological trends considered 3 different levels of significance (statistical analysis F-test): 1, 5 and 10%.

3. Results

3.1. Optimisation of the Extraction Method

The analysis conducted by comparing SOS, POS and EOS extracted from GPP with those extracted from the kNDVI index course (Figure 3) allowed the identification of reliable methodologies to assess phenological dates.

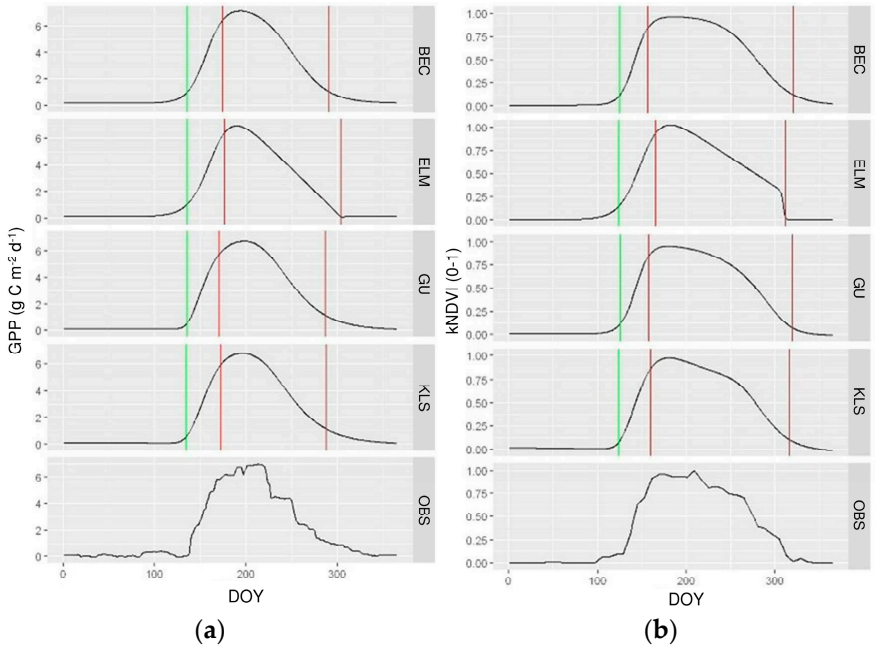

Figure 3. Example of SOS, POS and EOS extraction from GPP (**a**) and kNDVI (**b**) patterns of the Torgnon site (year 2017), with different fitting models: Becker (BEC), Elmore (ELM), Gu (GU), Klosterman (KLS)) and GU extraction. OBS represents the raw values of GPP and kNDVI. Vertical bars represent estimated SOS (green), POS (red) and EOS (dark red).

Regarding SOS, the FM×EM methodologies providing the best match between observed (i.e., GPP) and estimated data (i.e., kNDVI) were: ELM×$TRS_{0.3}$, GU×$TRS_{0.3}$ and BEC×$TRS_{0.4}$.

In the case of the peak of the season (POS), the use of the TRS extraction method was limited to one result, as this date was extracted from the maximum value reached by the

curve (TRS = 1). As shown in Table 3, the best results in POS calculation were obtained with ELM×GU and BEC×GU.

Table 3. Goodness of fit indicators between phenological dates extracted from GPP and kNDVI patterns with different FM×EM approaches. The results underlined and in bold are those relating to the approach chosen for the start (SOS) and peak (POS) of the season, respectively.

		SOS				POS				EOS			
		ELM	**GU**	**BEC**	**KLS**	**ELM**	**GU**	**BEC**	**KLS**	**ELM**	**GU**	**BEC**	**KLS**
GU	MAE	15.2	17.1	15.2	17.4	**13.4**	14.4	13.9	12.5	19.2	21.6	25.3	24.7
	R^2	0.76	0.74	0.75	0.83	**0.66**	0.62	0.54	0.56	0.08	0.06	0.00	0.05
	AIC	627	671	647	577	**647**	652	651	614	533	595	527	496
	RMSE	19.2	21.5	20.0	20.7	**18.5**	19.3	19.3	18.0	26.0	26.3	29.2	29.7
	pp	93	96	94	88	**91**	93	93	88	77	83	73	72
DER	MAE	15.0	16.9	14.2	12.6	16.2	28.6	23.8	16.8	18.8	35.8	39.5	36.3
	R^2	0.63	0.69	0.73	0.77	0.55	0.49	0.30	0.61	0.09	0.05	0.12	0.16
	AIC	682	668	674	568	512	480	530	416	557	498	560	479
	RMSE	21.1	21.9	17.8	16.3	21.1	34.6	30.2	23.7	25.4	40.6	43.1	40.1
	pp	95	95	99	86	73	64	69	56	79	69	80	72
KLS	MAE	17.4	15.0	13.9	19.5	10.3	15.8	13.9	13.6	22.6	23.3	24.1	27.1
	R^2	0.85	0.73	0.57	0.6	0.89	0.57	0.57	0.71	0.00	0.00	0.02	0.17
	AIC	116	300	582	505	110	345	582	431	104	222	458	351
	RMSE	21.5	18.2	19.0	24.0	13.1	22.2	19.0	19.3	33.1	29.5	28.65	32.7
	pp	17	46	83	69	16	47	83	60	16	30	64	47
$TRS_{0.1}$	MAE	15.4	19.4	21.0	19.2	16.2	28.5	23.8	16.8	21.1	21.5	22.9	24.4
	R^2	0.35	0.57	0.56	0.51	0.55	0.49	0.30	0.61	0.06	0.06	0.00	0.00
	AIC	635	612	651	598	512	480	530	416	589	302	325	235
	RMSE	19.3	24.1	25.7	24.3	21.06	34.6	30.2	23.7	26.5	26.0	28.0	30.0
	pp	91	83	94	81	73	64	69	56	84	46	48	33
$TRS_{0.2}$	MAE	14.0	14.8	13.6	15.8	-	-	-	-	22.8	21.9	24.9	25.9
	R^2	0.78	0.79	0.79	0.91	-	-	-	-	0.14	0.14	0.01	0.09
	AIC	609	611	625	497	-	-	-	-	588	498	583	459
	RMSE	17.7	19.7	17.6	19.5					28.3	27.0	30.4	30.2
	pp	91	89	94	75	-	-	-	-	85	72	80	68
$TRS_{0.3}$	MAE	**13.6**	15.0	12.9	14.6	-	-	-	-	27.5	29.4	28.9	31.6
	R^2	**0.82**	0.85	0.80	0.86	-	-	-	-	0.12	0.16	0.07	0.15
	AIC	**599**	593	627	553	-	-	-	-	588	547	548	529
	RMSE	**16.9**	19.0	16.2	17.9					32.0	33.8	33.9	35.8
	pp	**91**	90	95	86	-	-	-	-	85	79	78	78
$TRS_{0.4}$	MAE	13.7	14.9	12.8	13.3	-	-	-	-	34.2	36.1	35.5	36.6
	R^2	0.80	0.81	0.79	0.80	-	-	-	-	0.10	0.22	0.14	0.22
	AIC	629	624	626	580	-	-	-	-	569	574	545	522
	RMSE	18.1	19.3	15.9	16.7					38.4	39.4	39.1	39.8
	pp	94	93	95	88	-	-	-	-	83	83	79	78
$TRS_{0.5}$	MAE	13.7	15.7	13.3	12.6	-	-	-	-	39.8	42.0	40.3	40.3
	R^2	0.73	0.69	0.76	0.76	-	-	-	-	0.12	0.21	0.21	0.19
	AIC	652	674	648	566	-	-	-	-	523	567	527	505
	RMSE	18.6	20.5	17.1	16.7					43.5	45.0	43.1	43.6
	pp	94	95	96	84	-	-	-	-	75	81	78	74

The FMs reported are Elmore (ELM), Gu (GU), Beck (BEC) and Klosterman (KLS), the EMs Gu (GU), Derivatives (DER), Klosterman (KLS) and Threshold (TRS). Pp represents the percentage of points used for the evaluation (difference between dates extracted from GPP and kNDVI < 70 days).

The identification of EOS dates via remote sensing, on the other hand, was more problematic, with sub-optimal statistical values (R^2, MAE, AIC, RMSE) and a generally lower number of usable points after filtering with respect to SOS and POS (Table 3). Due to

the low performance in determining EOS through the kNDVI index, the end of the season was not considered in the analysis over the 2001–2021 period.

Among the methodologies that performed best in predicting SOS and POS, those chosen for the analysis of the period 2001–2021 were ELM×$TRS_{0.3}$ and ELM×GU, respectively. The choice fell on these two specific methodologies since for the extraction of start and peak dates, it was relevant to maintain the same type of fitting model (i.e., ELM), even if the extraction methods that worked better for SOS and POS were different ($TRS_{0.3}$ and GU for SOS and POS, respectively).

3.2. SOS and POS Trend Analysis (2001–2021)

The procedures selected during the methodological analysis (ELM×$TRS_{0.3}$ and ELM×GU, respectively, for SOS and POS) were used to investigate possible changes in the phenological timing of European grasslands. Given that from the results obtained in 3.1 (Table 3), the end of the season (EOS) was not well identified by MODIS-kNDVI when compared to EOS extracted from GPP, the analysis considered exclusively the start (SOS) and peak (POS) dates of the growing season.

Satellite-derived SOS showed a clear trend over the time span considered. As depicted in Table 4 and Figure 4, 26 sites (out of 31, i.e., 83.9% of the total) evidenced a negative correlation between SOS and years, indicating a progressive advance in the start of the growing season from 2001 onwards. From the SOS-years regression analysis, 17 grasslands sites showed a level of significance (F) < 0.1 in SOS anticipation. Specifically, 3 sites reported F values between 0.05 and 0.1 (AUS1, POL, RUS1), 5 between 0.01 and 0.05 (GEO, GER2, RUS2, SLV, TUR) and 9 < 0.01 (AUS2, BOS, CZE, DEN, FRA2, ITA3, HUN, SLK, SWI1).

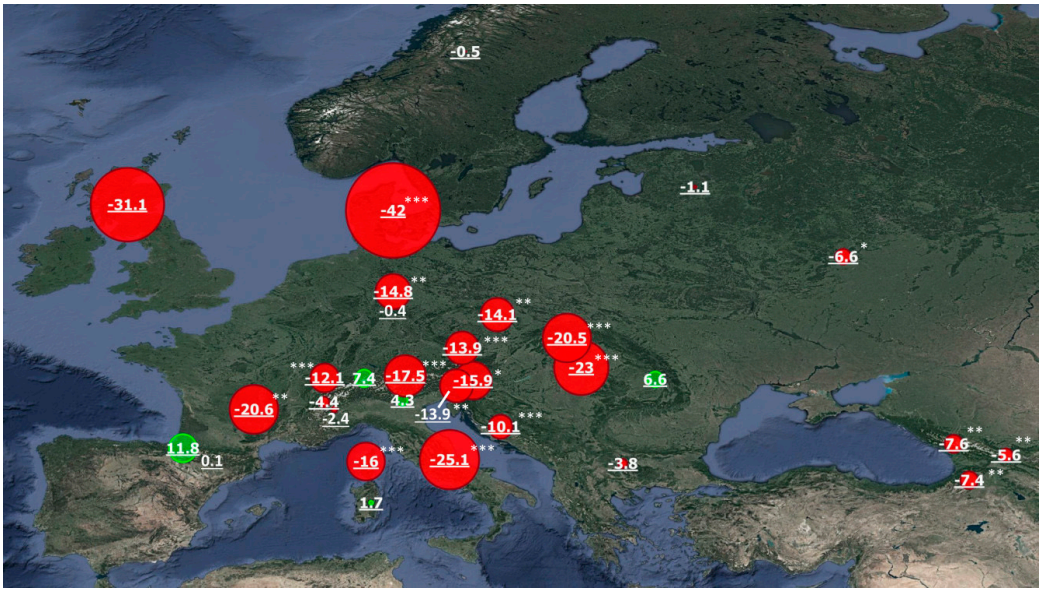

Figure 4. Changes (days) in SOS during the period 2001–2021. SOS advance is highlighted with red circles, whereas delay is highlighted with green circles. Sites that display a significant SOS-year correlation are marked with * ($0.05 < F \leq 0.1$), ** ($0.01 < F \leq 0.05$) and *** ($F \leq 0.01$).

The advance in SOS was subsequently quantified (Figure 4) by applying the equation identified from the specific SOS-years linear regression. From 2001 to 2021, the average advance of the growing season at significant sites ($F \leq 0.1$) was 15.92 days (0.76 days $year^{-1}$). However, it should be noted that the significant sites analysed showed different levels of SOS earliness, ranging for example from the 5.6-day advance of the RUS1 site to the 42.0-day advance of the DEN site.

As with SOS, the POS dates in the period 2001–2021 showed a trend towards an earlier peak of the grassland growing season. In fact, although in a smaller percentage than in SOS, 21 sites (67.7% of the total) evidenced an advance in POS dates (Table 4 and Figure 5).

Table 4. Results of SOS and POS analysis over the period 2001–2021. *Mean* represents the mean value of SOS and POS during the period 2001–2021, reported to give general information about each site (data not included in the analysis). *R* columns show the correlation coefficient (R) between phenological dates (i.e., SOS and POS) and years, *Sign*. the significance (F) of the SOS and POS-years regression, and *Days* the difference between SOS and POS in the years 2001 and 2021 according to the equation found with the linear regression.

	SOS					POS				
ID	**Mean**	**R**	**Days**	**Sign.**	**Pp**	**Mean**	**R**	**Days**	**Sign.**	**Pp**
AUS1	139.32	−0.43	**−15.89**	**0.06**	0.9	169.35	−0.25	−4.54	0.3	0.95
AUS2	159.3	−0.66	**−17.51**	**<0.01**	0.95	187.16	−0.52	**−14.02**	**0.03**	0.9
BOS	116.05	−0.68	**−10.08**	**<0.01**	0.9	157.52	−0.4	**−9.93**	**0.09**	1
BUL	172.7	−0.17	−3.77	0.48	0.95	197.9	−0.11	−5.53	0.65	0.95
CZE	85.16	−0.66	**−13.88**	**<0.01**	0.9	129.68	−0.52	**−17.2**	**0.02**	0.9
DEN	91.63	−0.74	**−42**	**<0.01**	0.86	124.18	−0.44	**−14.31**	**0.06**	0.81
FRA1	124.3	−0.34	−4.42	0.15	0.95	154.19	0.5	**4.44**	**0.03**	0.95
FRA2	94.47	−0.61	**−20.6**	**<0.01**	0.9	140.42	−0.4	**−6.66**	**0.09**	0.9
FRA3	97.5	−0.61	**−15.99**	**<0.01**	0.95	130.85	−0.12	−3.57	0.64	0.95
GEO	148.95	−0.47	**−5.55**	**0.04**	0.95	177.65	−0.4	**−7.42**	**0.1**	0.95
GER1	84.75	−0.01	−0.42	0.96	0.76	117.67	−0.15	−5.47	0.53	0.86
GER2	99.05	−0.48	**−14.76**	**0.04**	0.9	131.48	−0.62	**−27.73**	**<0.01**	1
HUN	69.23	−0.65	**−22.95**	**<0.01**	0.65	154.11	0	−12.02	0.74	0.95
ITA1	138.84	−0.07	−2.42	0.77	0.9	167.9	0.17	4.51	0.49	0.95
ITA2	136.95	0.22	4.3	0.36	0.95	165.65	0.5	**6.8**	**0.03**	0.95
ITA3	11.56	−0.77	**−25.14**	**<0.01**	0.86	143	0.22	5.28	0.36	0.95
ITA4	107.35	0.08	1.71	0.73	0.81	128.05	−0.2	−5.74	0.41	1
LAT	113.11	−0.11	−1.12	0.65	0.9	146.35	−0.89	**−27.1**	**<0.01**	0.95
POL	102.58	−0.43	**−14.06**	**0.07**	0.9	138.8	−0.4	**−10.82**	**0.09**	0.95
ROM	128	0.22	6.64	0.38	0.95	166.85	0.07	1.58	0.78	0.95
RUS1	119.26	−0.39	**−6.56**	**0.1**	0.9	149.94	−0.24	−6.37	0.33	0.81
RUS2	148	−0.52	**−7.59**	**0.02**	0.95	181.76	−0.64	**−13.49**	**<0.01**	1
SCO	125.2	−0.34	−31.05	0.16	0.95	161.39	0.13	7.21	0.61	0.86
SLK	122.76	−0.66	**−20.52**	**<0.01**	0.81	157.82	0.37	17.35	0.18	0.81
SLV	130	−0.54	**−13.89**	**0.02**	0.86	164.25	−0.4	**−8.3**	**0.09**	0.9
SPA1	88.28	0.32	11.75	0.18	0.9	155.21	0.37	15.1	0.12	0.9
SPA2	125.67	0	−0.05	0.99	1	154.89	−0.24	−3.86	0.32	0.9
SWE	172.21	−0.02	−0.5	0.94	0.9	191.53	−0.55	**−19.62**	**0.02**	0.9
SWI1	110.35	−0.7	**−12.11**	**<0.01**	0.95	135.04	0.19	3.78	0.44	0.95
SWI2	124.6	0.32	7.37	0.17	0.95	152.86	−0.33	−11.51	0.17	1
TUR	151.8	−0.55	**−7.4**	**0.02**	0.95	185.9	−0.55	**−9.54**	**<0.01**	0.95

Pp is the percentage of points used out of the total after the filtering procedure. Results with significance <0.1 are shown in bold.

From POS-years regression analysis, 13 grassland sites showed a level of significance (F) of < 0.1 in POS advance during the period 2001–2021. Specifically, 6 sites reported F values between 0.05 and 0.1 (BOS, DEN, FRA2), 3 between 0.01 and 0.05 (AUS2, CZE, SWE) and 4 < 0.01 (GER2, LAT, RUS2, TUR). In the case of POS, in addition to sites that showed a significant advance in the beginning of the season, two sites highlighted contrasting trends (FRA1 and ITA2), showing a clear delay in the peak of the season ($0.01 < F < 0.05$). As for SOS, changes in phenological dates during the period 2001–2021 were quantified for each site (Figure 5). Considering all the significant sites ($F \leq 0.1$), including those that showed a delay, the average advance in the peak of the growing season was 11.66 days (0.56 days year^{-1}).

In order to carry out an assessment of temperature influence in determining the phenological dates of European grasslands over the 2001–2021 period, statistical analyses were performed to assess the temperature trend over the years considered and the impacts of thermal factors on SOS and POS. From the results of the linear regressions performed between temperatures and years (Table 5), the mean winter temperatures showed an increasing trend in 21 of the 23 sites (sites with no or little weather data were excluded),

corresponding to 91.30% of the total. Of these, 16 (69.57%) showed a significant change ($F < 0.1$) over the time period analysed. On the other hand, the average spring temperatures showed a less homogenous trend, with a lower tendency of temperature increase (65.21%) and fewer sites (6) with significant change (26.08%).

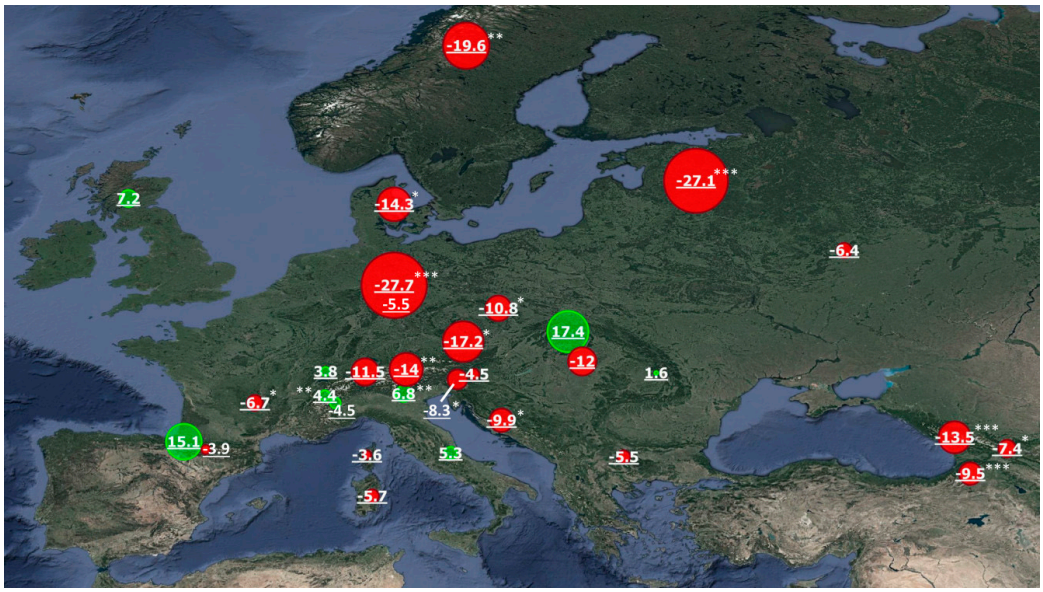

Figure 5. Changes (days) in POS during the period 2001–2021. SOS advance is highlighted with red circles, whereas delay is highlighted with green circles. Sites that display a significant POS-year correlation are marked with * ($0.05 < F \leq 0.1$), ** ($0.01 < F \leq 0.05$) and *** ($F \leq 0.01$).

Table 5. Results of the statistical analysis conducted on weather data from 2001 to 2021. *R years* highlights temperature trends over the 2001–2021 period by reporting the values of the correlation coefficients found by correlating the average winter and spring temperatures with the reference years, while *R SOS* and *R POS* report the values found by comparing the extracted SOS and POS with the average winter and spring temperatures of the respective years. For each comparison, the level of significance F is reported (*Sign.*). *T mean* values represent the mean temperatures of the winter and spring seasons, reported to give general information about each site (data not included in the analysis).

	Winter					Spring						
ID	**T Mean**	**R Years**	**Sign.**	**R SOS**	**Sign.**	**T Mean**	**R Years**	**Sign.**	**R SOS**	**Sign.**	**R POS**	**Sign.**
AUS1	1.12	0.78	**<0.01**	−0.51	**0.09**	13.93	−0.11	0.74	−0.41	0.19	−0.22	0.5
AUS2	−4.15	0.72	**<0.01**	−0.36	0.16	5.9	0	0.99	−0.03	0.91	−0.52	**0.03**
BOS	3.73	0.74	**<0.01**	−0.63	**0.01**	16.1	0.62	**0.01**	−0.61	**0.01**	−0.64	**0.01**
BUL	−9.07	0.68	**<0.01**	−0.28	0.25	−0.22	0.47	**0.04**	−0.16	0.51	0.18	0.45
CZE	1.73	0.66	**<0.01**	−0.55	**0.02**	13.82	0.33	0.18	-	-	−0.3	0.23
DEN	2.16	0.72	**<0.01**	−0.64	**<0.01**	11.44	0.76	**<0.01**	−0.29	0.24	−0.62	**<0.01**
FRA1	2.33	0.56	**0.01**	−0.27	0.27	13.79	0.05	0.84	−0.57	**0.01**	−0.06	0.82
FRA2	4	0.36	0.13	−0.67	**<0.01**	12.93	−0.24	0.32	−0.17	0.48	0.09	0.72
FRA3	10.82	0.65	**<0.01**	−0.08	0.75	18.07	0.11	0.65	0.09	0.71	−0.49	**0.03**
GEO	0.06	0.25	0.43	0.02	0.95	13.22	−0.01	0.97	−0.29	0.34	0.15	0.62
GER1	1.91	0.46	**0.08**	−0.03	0.91	12.92	0.24	0.39	-	-	−0.41	0.13
GER2	2.77	0.3	0.21	0	1	13.15	0.12	0.63	−0.32	0.18	0	0.99
HUN	2.26	0.61	**0.01**	−0.31	0.27	16.45	0.36	0.13	-	-	0.04	0.87
ITA1 [a]	−0.24	-	-	-	-	9.46	-	-	-	-	-	-
ITA2	−3.83	0.1	0.67	0.02	0.93	4.94	−0.36	0.13	−0.04	0.88	−0.16	0.52
ITA3 [b]	-	-	-	-	-	-	-	-	-	-	-	-
ITA4	8.17	0.67	**0.01**	0.32	0.27	17.48	−0.07	0.82	−0.35	0.22	−0.56	**0.04**
LAT	−3.92	0.53	**0.04**	−0.52	**0.05**	10.8	0.51	**0.05**	−0.53	**0.04**	−0.55	**0.03**
POL	−0.32	0.53	**0.02**	−0.32	0.18	12.32	0.23	0.34	−0.57	**0.01**	−0.55	**0.02**
ROM [a]	1.88	-	-	-	-	15.02	-	-	-	-	-	-
RUS1	−3.57	0.48	**0.04**	−0.33	0.17	14.09	0.44	**0.06**	−0.28	0.25	−0.74	**<0.01**
RUS2 [a]	1.24	-	-	-	-	11.53	-	-	-	-	-	-

Table 5. *Cont.*

	Winter					Spring						
ID	**T Mean**	**R Years**	**Sign.**	**R SOS**	**Sign.**	**T Mean**	**R Years**	**Sign.**	**R SOS**	**Sign.**	**R POS**	**Sign.**
SCO	1.22	−0.37	0.12	−0.18	0.47	6.71	0.24	−0.31	−0.14	0.56	−0.47	**0.05**
SLK [b]	-	-	-	-	-	-	-	-	-	-	-	-
SLV [a]	−0.25	-	-	-	-	11.69	-	-	-	-	-	-
SPA1	7.08	−0.11	0.66	0.08	0.74	15.48	−0.87	**<0.001**	-	-	−0.45	**0.05**
SPA2 [b]	-	-	-	-	-	-	-	-	-	-	-	-
SWE	−8.69	0.03	0.89	0.24	0.34	1	−0.34	0.17	−0.69	**<0.00**	−0.2	0.43
SWI1	−0.1	0.63	**<0.001**	−0.56	**0.02**	9.37	0.17	0.51	−0.46	**0.06**	−0.15	0.55
SWI2	0.15	0.52	**0.02**	0.01	0.97	10.51	0.03	0.92	−0.16	0.51	−0.02	0.92
TUR [a]	−3.43	-	-	-	-	13.17	-	-	-	-	-	-

Site names with [a] and [b] represent the sites with insufficient ([a]) or no ([b]) weather data to conduct the analysis. Results with significance <0.1 are shown in bold.

The results on the influence of winter and spring temperatures on SOS, showed a negative correlation between SOS and temperatures, significant in 7 sites (F < 0.1, AUS1, BOS, CZE, DEN, FRA2, LAT, SWI1) with winter temperature and in 6 (BOS, FRA1, LAT, POL, SWE, SWI1) with spring temperature as the main driver.

Since POS always occurred several weeks after winter's end, in the analysis we considered only the effect of spring temperatures. Here, too, the relationship highlighted a negative correlation between phenological dates (i.e., POS) and temperature. In particular, 10 sites (AUS2, BOS, DEN, FRA3, ITA4, LAT, POL, RUS1, SCO, SPA1) showed a significance F in the POS-spring temperature relationship of less than 0.1.

Taking into account the grasslands where the change was significant at both the SOS and POS dates (11 sites), we investigated the influence of two other potential phenological season variables: the latitude and altitude of the test sites. As can be seen in Figure 6, the change in advance during the period 2001–2021 is greater with increasing latitude for both SOS and POS, with the former showing a higher correlation (R = −0.81) than the latter (R = −0.55). Observing the correlations between changes in phenological dates and altitude, sites at higher altitudes show less advance in SOS and POS than those at lower altitudes. As in the case of the SOS and POS-latitude correlation, the absolute values of R are greater for the change in SOS dates (R = 0.69) than for POS (R = 0.36).

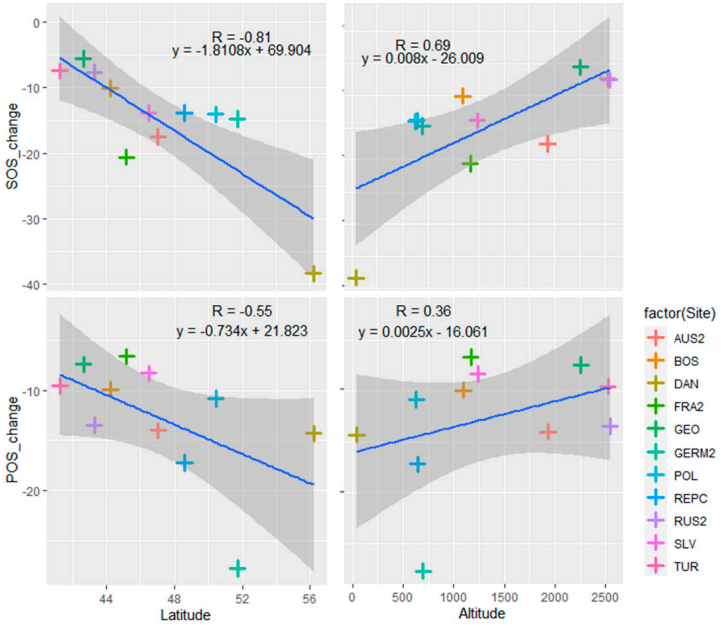

Figure 6. SOS and POS changes during the period 2001–2021 compared with the latitude and altitude of the sites where changes are significant in both SOS and POS.

In addition to the analysis of the changes that occurred in SOS and POS over the reference period, changes in the duration of the timeframe between SOS and POS (i.e., SOS-POS duration) were also analysed (Figure 7).

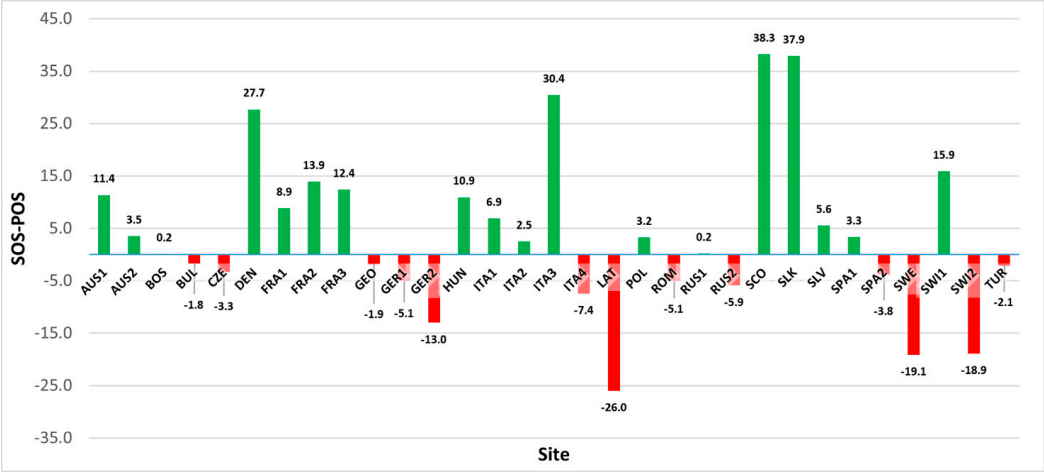

Figure 7. Changes in SOS-POS (number of days) interval during the period 2001–2021 for all test sites.

The data did not show any common trend within the framework of the European grasslands analysed. Indeed, within the dataset considered, some sites showed an increase in the SOS-POS duration (56.67%), while others showed a decrease (43.33%). The lengthening of the SOS-POS duration between 2001 and 2021 was determined by a less marked anticipation of the POS with respect to the SOS (e.g., DEN) or the postponement of the former (e.g., FRA1). The reduction in the SOS-POS duration, on the other hand, was generally caused by a higher advance in POS than in SOS (e.g., GER2).

The change in the time duration of the SOS-POS interval was also analysed in the light of the individual changes in SOS dates. Figure 8 depicts the change in the SOS-POS interval, showing an increase in the number of days as the magnitude of the SOS advance grows and highlighting the influence of an advanced SOS on the lengthening of SOS-POS duration. The analysis was also conducted considering three different levels of altitudinal and latitudinal ranges, but no clear trends emerged.

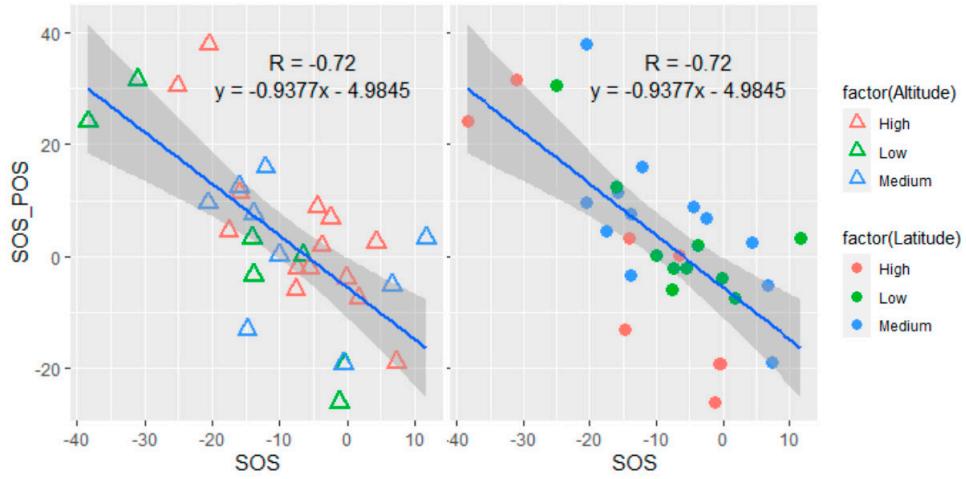

Figure 8. Relationships between changes in SOS-POS duration and changes in SOS during the period 2001–2021. Figures represent the same equation, highlighting sites graphically according to altitude (left) or latitude (right). Sites are divided into 3 different classes of altitude (low, 0–650 m; medium, 650–1300 m; high +1300 m) and latitude (low, 40–45°; medium, 45–50°; high +50°).

Figure 9 shows an example of the trend in average temperatures for the 30 days following the SOS at the DEN site, highlighting how an earlier SOS date results in a generally colder initial growing season, which can lead to a delay in the POS date and a lengthening of the SOS-POS duration (e.g., DEN). Although colder average temperatures are generally present when the start of the season occurs early, the lengthening of the SOS-POS duration, visible for example at the DEN site, was not always visible at all test sites (e.g., Figure 7), likely due to different grass species.

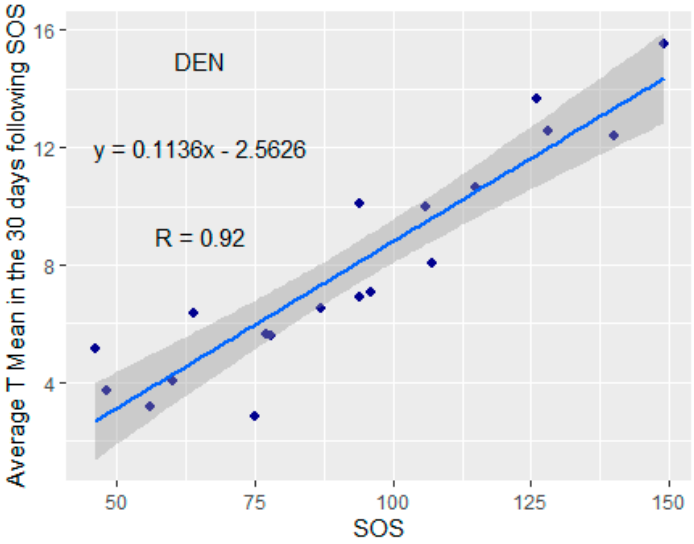

Figure 9. Example of relationships between SOS and the mean temperature of the 30 days after SOS at the DEN site.

4. Discussion

This study aimed to identify the best methodology for the estimation of phenological dates through satellite-processed vegetation indices. As in other studies [26,27], GPP measurements were used to extract SOS, POS and EOS as observed data to be compared with those elaborated from kNDVI patterns. Due to the valuable relationship between kNDVI and GPP found for grasslands in [47], the use of this index enabled phenological dates (i.e., SOS and POS) to be estimated in agreement with those extracted by GPP patterns at sites endowed with eddy covariance flux towers. Various fitting models and extraction methods were tested and evaluated in our study, providing different results for SOS, POS and EOS detection. For consistency, a trend analysis was performed by deploying only one fitting model (i.e., ELM) among those selected. Then, we identified the best extraction method for each specific phenological date (i.e., $TRS_{0.3}$ and GU for SOS and POS, respectively). It is important to underline that the fitting model (i.e., the curve that fits kNDVI points and from which dates are extracted) is the same in all trend analyses (i.e., SOS and POS) and for all sites and years. The choice to use different extraction methods on the same curve for SOS and POS derived from the results obtained in Section 3.1. Although it was more coherent to select only one method, we decided to select the most robust extraction methods for each phenological date (i.e., SOS and POS) in order to achieve more precision in SOS and POS estimation during the analysis of the 2001–2021 period. In fact, using the same extraction method could determine greater errors, since, for example, one method can be optimal for SOS but sub-optimal for POS estimation. SOS and POS dates extracted from kNDVI were in line with those estimated from GPP, even if some uncertainties were still present, as seen from MAE (13.6 and 13.4 days, respectively for SOS and POS) and RMSE values (16.9 and 18.5 days, respectively for SOS and POS). EOS, conversely, proved to be more difficult to detect than SOS and POS. This is confirmed by Tian et al. [15], who achieved lower levels of accuracy in estimating EOS in different environments, and by Zheng and Zhu [53], who observed large differences

and poor correlation between EOS extracted from satellite vegetation indices and ground-observed EOS in a specific study on grasslands. Differently from Tian et al. [15] and Gonsamo et al. [14] for forests and croplands, in this study the estimation of EOS from satellites did not reach a level of accuracy that can provide a reliable analysis for EOS trends over the period 2001–2021. However, it should also be noted that the extraction of SOS and EOS dates in grasslands is subject to greater uncertainties than in other environments, such as deciduous-broadleaf and mixed forests [54]. Leaf senescence responses in herbaceous species are influenced by several meteorological variables, with a complex dependence on species, functional types and geographical gradients [55]. Differences in scale and content (spectral response and phenological event) between satellite-derived and ground-observed phenology can result in discrepancies between satellite-derived phenological dates and changes in leaf colouring, although these measurements are related (e.g., EOS and the beginning of leaf colouring) [56–58]. This is especially noticeable for EOS. In fact, the change in canopy greenness is slower and longer in autumn with respect to spring [59,60], thus causing a reduced variability in EOS compared to SOS and a greater difficulty in detecting the end of season from satellite [15,53].

From our trend analysis, the European grasslands analysed showed a general advance in the start (SOS) and peak of the season (POS) over the 2001–2021 time period. This anticipation is in agreement with what was observed in different time frames in both grassland [37,61–64] and non-grassland biomes in Europe [36,38]. Specifically, in our study, SOS and POS advance in significant sites (Table 4) was 0.76 days year^{-1} and 0.56 days year^{-1}, respectively for the 2001–2021 period. In some cases, however, an opposite trend was observed, i.e., a slight tendency to delay in the SOS and/or POS dates. This could be partially explained for SOS and, consequently POS, by an insufficient cooling effect due to warming conditions in late autumn or winter [61]. On the other hand, as regards the POS only, the anticipation of SOS in response to increasing temperatures may shift the following SOS-POS duration to colder environmental conditions (e.g., Figure 9), which in turn may lead in some cases to a progressive lengthening of SOS-POS durations. This is in agreement with the modelling exercise of Sadras and Monzon [65], who suggested that an earlier flowering in wheat due to temperature increase during the period 1971–2000 may have determined shifts in post-flowering development at lower temperatures, neutralising the trend of increasing temperatures and leaving post-flowering phase duration unchanged. The same was observed in the field of grapevine [66]. This could explain part of our results regarding SOS-POS duration, particularly for those sites showing a lengthening. However, the trend is not evident in all the grassland sites analysed in this study, as a certain number of sites (i.e., 13) showed a shortening of the SOS-POS length. These outcomes result from a not too marked SOS anticipation (e.g., LAT, SWE, SWI2) and a consequent relapse of SOS into a time range (i.e., DOY) similar to the ones observed at the turn of the year 2001. In addition, the generally higher temperatures (i.e., global warming) and, probably, less water availability occurring after each specific SOS probably caused an advance in the vegetation peak [67,68], inducing a shortening in SOS-POS duration, as the SOS remains unchanged and the POS is advanced. The presence of a spurious bias in SOS-POS length deriving from the different extraction methods for SOS and POS in estimating SOS-POS length is possible. However, investigating SOS-POS length per se was not our final goal, since our attention was mainly focused on trends. In fact, if a bias was present, this error did not influence the trend analysis, as it was present in the same way in all years from which SOS and POS were extracted.

The study of seasonal average temperatures (i.e., winter and spring) showed a general rise in temperatures across Europe for the period 2001–2021, resulting in a negative correlation, significant in some cases (Table 5), with SOS and POS dates. Summer and autumn temperatures were not considered since EOS, the phenological date that occurs after these seasons, was excluded from the trend analysis since satellite estimations were not sufficiently reliable.

The effect of temperature was found to be a decisive factor in the change of phenological dates of SOS and POS, in agreement with Ganjurjav et al. [69] and Ren et al. [63], also influencing phenology spatially [70]. Consequently, the rise in temperatures recorded in the 2001–2021 time frame could also have had an indirect effect on the advancement of the SOS date by causing an advancement in the snowmelt dates recorded in recent years [71], without the risk of increasing frost exposure [72]. Snow melt and snow cover are indeed decisive in determining the length of the growing season and the phenological development of high-altitude and high-latitude grasslands [73,74], also influencing water availability or thermal conditions by soil insulation [75]. However, according to Xie et al. [76], in a specific study on the European Alps, spring temperature was the predominant factor in SOS advancement, while snow cover and snow melt, although important, played a secondary role.

Temperature is therefore an important factor, but our results often do not show a significant relationship between this parameter and SOS and POS (Table 5). This can be explained by the fact that, in addition to temperature, there are other factors that may influence phenological dates, such as CO_2 concentration, the presence of nitrogen in soil, solar radiation, wind speed, atmospheric pressure, snow cover or precipitation [67,68]. Snow cover for instance, as reported in Jerome et al. [77], can act through temperature accumulation but also independently as a driver of plant phenology. Regarding precipitation, Xu et al. [78] observed an earlier onset of the grassland growing season due to higher temperatures only when water was not a limiting factor, with a non-linear response. In contrast, Hua et al. [68] pointed out that high precipitation can have a delaying effect on the peak season (POS) as a result of the high correlation between this phenological stage and rainfall.

Our study highlighted the influence of altitudinal and latitudinal conditions on the phenological stages of grassland with significant changes ($F \leq 0.1$) in SOS and POS during 2001–2021. Correlations between the magnitude of change in SOS and altitude and latitude indicated higher absolute values than the respective correlations with POS. The sites that showed higher changes in the dates of SOS and, to a lesser extent, POS were those located at higher latitudes and lower altitudes (e.g., DEN, 56.1995°N, 40 m a.s.l.), while at low latitudes and high altitudes (e.g., TUR, 41.2610°N, 2524 m a.s.l.) showed smaller phenological changes.

The contrasting behaviour of changes (i.e., advances and/or postponement) in SOS and POS dates can also be explained by the variability in botanical composition as a result of the different environments in which the study sites are located. This is confirmed by several studies [55,79–82] that highlight the importance of species or functional types on the phenological stages of plants. In addition, as observed by Cleland et al. [67], diverse plant functional types have different phenological changes in response to multiple environmental factors (e.g., CO_2 concentration or soil resources). Moreover, the changes in temperatures recorded over the last few decades, beyond having a direct effect on the early or late season, may have influenced the change in the composition of functional groups [83], which in turn may alter the grassland phenological stages. Nevertheless, the main aim of our work was to highlight general trends in phenology, without a particular focus on the species present in the test areas. Given the spatial-temporal extent of the trend analysis, reliable and timely information on the specific botanical composition at the 31 study sites over the years of investigation was, moreover, difficult to obtain. Indications regarding phenological responses of different species can, however, also be gathered indirectly from observing the results in Figure 6, which analyses the phenological changes observed at different altitudinal and latitudinal gradients, conditions that reflect the type of vegetation that may be present in those environments.

Although investigating the phenology of different species was not our main objective, knowing the type of species or functional groups present would have provided useful information to increase understanding of the results. In fact, as explained above, this information may clarify the contrasting results obtained for some study sites. Nevertheless, the results showed a clear general tendency of grassland phenology to advance, especially the SOS date.

Overall, our results confirmed what was already observed in a sparse and limited number of EU countries [36] and under a different time span in Europe [38], while remaining in line with other studies in other areas of the world [61,68]. The analysis conducted with an exclusive focus on the grassland environment provides important indications of both the extent of these phenological changes and their distribution within the European continent, as well as the influence of increasing temperatures.

The phenological estimates obtained from MODIS satellite data over the time period 2001–2021 represent key information for understanding the evolution of grassland phenology that has occurred in recent years and the trend towards which it is heading, providing policy makers and stakeholders with useful indications for the identification of possible adaptation and mitigation strategies.

Despite the uncertainties, the methodology presented in this paper can represent a first step in a European-wide assessment of grassland phenology, opening up the possibility of investigating phenological trends over large and numerous grassland areas of the continent. Concerning future perspectives, a specific end-of-season study could be important to reduce uncertainties in EOS detection from satellites and refine the methodology. In addition, the analysis performed can be extended by focusing on the differences that may occur in grasslands characterised by the presence of different dominant species and groups. The analysis of the factors driving the phenological changes can also be extended to water conditions (i.e., precipitation and snowmelt date) in the case of high-quality data over an extended period of time.

5. Conclusions

This study provided important information on the phenology of European grasslands. kNDVI resulted in being a reliable vegetation index for estimating the phenological dates of SOS and POS, but the same effectiveness cannot be applied to EOS. The analysis of MODIS satellite data from 2001 to 2021 showed a clear trend towards an earlier start to the growing season (SOS) across Europe. An advance in the date of the peak season (POS) is also evident, although generally less marked and, in some cases, even delayed than at the beginning of the reference period of analysis. The seasonal average temperature (i.e., winter and spring) was generally found to be increasing at all sites, often proving to be a significant driver of the advancement of grassland phenological dates over the European domain. Analyses conducted with a specific focus on grasslands have provided very important insights into the status of these systems throughout Europe and the evolution, in phenological terms, that they have been undergoing in recent decades.

Author Contributions: Conceptualization, E.B. and M.M.; methodology, M.G., G.F., E.B. and M.M.; software, G.F.; validation, E.B., L.L. and L.S.; formal analysis, E.B., C.D., L.S. and L.L.; investigation, E.B. and G.A.; resources, C.D. and G.A.; Data Curation, E.B., N.S. and L.S.; Writing–Original Draft Preparation, E.B.; writing–review and editing, M.M., G.A., C.D., M.G., G.F., N.S., L.S. and L.L; visualization, E.B. and M.M.; supervision, M.M. and G.A.; project administration, C.D.; funding acquisition, C.D. All authors have read and agreed to the published version of the manuscript.

Funding: This research received no external funding.

Data Availability Statement: Not applicable.

Acknowledgments: Research partially supported by the project "Unraveling interactions between WATER and carbon cycles during drought and their impact on water resources and forest and grassland ecosySTEMs in the Mediterranean climate (WATERSTEM)", financed by the Italian Ministry of University and Research.

Conflicts of Interest: The authors declare no conflict of interest.

References

1. Lieth, H. *Phenology and Seasonality Modeling*; Springer: New York, NY, USA, 1974.
2. Richardson, A.D.; Keenan, T.F.; Migliavacca, M.; Ryu, Y.; Sonnentag, O.; Toomey, M. Climate Change, Phenology, and Phenological Control of Vegetation Feedbacks to the Climate System. *Agric. For. Meteorol.* **2013**, *169*, 156–173. [CrossRef]

3. Singh, R.K.; Svystun, T.; AlDahmash, B.; Jönsson, A.M.; Bhalerao, R.P. Photoperiod- and Temperature-Mediated Control of Phenology in Trees—A Molecular Perspective. *New Phytol.* **2017**, *213*, 511–524. [CrossRef] [PubMed]
4. Templ, B.; Koch, E.; Bolmgren, K.; Ungersböck, M.; Paul, A.; Scheifinger, H.; Rutishauser, T.; Busto, M.; Chmielewski, F.M.; Hájková, L.; et al. Pan European Phenological Database (PEP725): A Single Point of Access for European Data. *Int. J. Biometeorol.* **2018**, *62*, 1109–1113. [CrossRef] [PubMed]
5. Cui, T.; Martz, L.; Lamb, E.G.; Zhao, L.; Guo, X. Comparison of Grassland Phenology Derived from MODIS Satellite and PhenoCam Near-Surface Remote Sensing in North America. *Can. J. Remote Sens.* **2019**, *45*, 707–722. [CrossRef]
6. Liu, Y.; Hill, M.J.; Zhang, X.; Wang, Z.; Richardson, A.D.; Hufkens, K.; Filippa, G.; Baldocchi, D.D.; Ma, S.; Verfaillie, J.; et al. Using Data from Landsat, MODIS, VIIRS and PhenoCams to Monitor the Phenology of California Oak/Grass Savanna and Open Grassland across Spatial Scales. *Agric. For. Meteorol.* **2017**, *237–238*, 311–325. [CrossRef]
7. Dixon, D.J.; Callow, J.N.; Duncan, J.M.A.; Setterfield, S.A.; Pauli, N. Satellite Prediction of Forest Flowering Phenology. *Remote Sens. Environ.* **2021**, *255*, 112197. [CrossRef]
8. Peng, D.; Wang, Y.; Xian, G.; Huete, A.R.; Huang, W.; Shen, M.; Wang, F.; Yu, L.; Liu, L.; Xie, Q.; et al. Investigation of Land Surface Phenology Detections in Shrublands Using Multiple Scale Satellite Data. *Remote Sens. Environ.* **2021**, *252*, 112133. [CrossRef]
9. Migliavacca, M.; Galvagno, M.; Cremonese, E.; Rossini, M.; Meroni, M.; Sonnentag, O.; Cogliati, S.; Manca, G.; Diotri, F.; Busetto, L.; et al. Using Digital Repeat Photography and Eddy Covariance Data to Model Grassland Phenology and Photosynthetic CO_2 Uptake. *Agric. For. Meteorol.* **2011**, *151*, 1325–1337. [CrossRef]
10. Julitta, T.; Cremonese, E.; Migliavacca, M.; Colombo, R.; Galvagno, M.; Siniscalco, C.; Rossini, M.; Fava, F.; Cogliati, S.; Morra di Cella, U.; et al. Using Digital Camera Images to Analyse Snowmelt and Phenology of a Subalpine Grassland. *Agric. For. Meteorol.* **2014**, *198–199*, 116–125. [CrossRef]
11. Zhang, X.; Jayavelu, S.; Liu, L.; Friedl, M.A.; Henebry, M.; Liu, Y.; Schaaf, C.B.; Richardson, A.D.; Gray, J. Evaluation of Land Surface Phenology from VIIRS Data Using Time Series of PhenoCam Imagery. *Agric. For. Meteorol.* **2018**, *256–257*, 137–149. [CrossRef]
12. Watson, C.J.; Restrepo-Coupe, N.; Huete, A.R. Multi-Scale Phenology of Temperate Grasslands: Improving Monitoring and Management with Near-Surface Phenocams. *Front. Environ. Sci.* **2019**, *7*, 1–18. [CrossRef]
13. Sonobe, R.; Yamaya, Y.; Tani, H.; Wang, X.; Kobayashi, N.; Mochizuki, K. Crop Classification from Sentinel-2-Derived Vegetation Indices Using Ensemble Learning. *J. Appl. Remote Sens.* **2018**, *12*, 1. [CrossRef]
14. Gonsamo, A.; Chen, J.M.; David, T.P.; Kurz, W.A.; Wu, C. Land Surface Phenology from Optical Satellite Measurement and CO_2 Eddy Covariance Technique. *J. Geophys. Res. Biogeosciences* **2012**, *117*, 1–18. [CrossRef]
15. Tian, F.; Cai, Z.; Jin, H.; Hufkens, K.; Scheifinger, H.; Tagesson, T.; Smets, B.; Van Hoolst, R.; Bonte, K.; Ivits, E.; et al. Calibrating Vegetation Phenology from Sentinel-2 Using Eddy Covariance, PhenoCam, and PEP725 Networks across Europe. *Remote Sens. Environ.* **2021**, *260*, 112456. [CrossRef]
16. Lara, B.; Gandini, M. Assessing the Performance of Smoothing Functions to Estimate Land Surface Phenology on Temperate Grassland. *Int. J. Remote Sens.* **2016**, *37*, 1801–1813. [CrossRef]
17. Filippa, G.; Cremonese, E.; Migliavacca, M.; Galvagno, M.; Forkel, M.; Wingate, L.; Tomelleri, E.; Morra di Cella, U.; Richardson, A.D. Phenopix: A R Package for Image-Based Vegetation Phenology. *Agric. For. Meteorol.* **2016**, *220*, 141–150. [CrossRef]
18. Gitelson, A.A.; Viña, A.; Verma, S.B.; Rundquist, D.C.; Arkebauer, T.J.; Keydan, G.; Leavitt, B.; Ciganda, V.; Burba, G.G.; Suyker, A.E. Relationship between Gross Primary Production and Chlorophyll Content in Crops: Implications for the Synoptic Monitoring of Vegetation Productivity. *J. Geophys. Res. Atmos.* **2006**, *111*, 1–13. [CrossRef]
19. Running, S.W.; Nemani, R.R.; Heinsch, F.A.; Zhao, M.; Reeves, M.; Hashimoto, H. A Continuous Satellite-Derived Measure of Global Terrestrial Primary Production. *Bioscience* **2004**, *54*, 547–560. [CrossRef]
20. Wang, J.; Wu, C.; Zhang, C.; Ju, W.; Wang, X.; Chen, Z.; Fang, B. Improved Modeling of Gross Primary Productivity (GPP) by Better Representation of Plant Phenological Indicators from Remote Sensing Using a Process Model. *Ecol. Indic.* **2018**, *88*, 332–340. [CrossRef]
21. Fu, Y.S.H.; Campioli, M.; Vitasse, Y.; De Boeck, H.J.; Van Den Berge, J.; AbdElgawad, H.; Asard, H.; Piao, S.; Deckmyn, G.; Janssens, I.A. Variation in Leaf Flushing Date Influences Autumnal Senescence and Next Year's Flushing Date in Two Temperate Tree Species. *Proc. Natl. Acad. Sci. USA* **2014**, *111*, 7355–7360. [CrossRef]
22. Zhang, Q.; Cheng, Y.-B.; Lyapustin, A.I.; Wang, Y.; Xiao, X.; Suyker, A.; Verma, S.; Tan, B.; Middleton, E.M. Estimation of Crop Gross Primary Production (GPP): I. Impact of MODIS Observation Footprint and Impact of Vegetation BRDF Characteristics. *Agric. For. Meteorol.* **2014**, *191*, 51–63. [CrossRef]
23. Peng, D.; Zhang, X.; Wu, C.; Huang, W.; Gonsamo, A.; Huete, A.R.; Didan, K.; Tan, B.; Liu, X.; Zhang, B. Intercomparison and Evaluation of Spring Phenology Products Using National Phenology Network and AmeriFlux Observations in the Contiguous United States. *Agric. For. Meteorol.* **2017**, *242*, 33–46. [CrossRef]
24. Medlyn, B.E. Physiological Basis of the Light Use Efficiency Model. *Tree Physiol.* **1998**, *18*, 167–176. [CrossRef] [PubMed]
25. Galvagno, M.; Wohlfahrt, G.; Cremonese, E.; Rossini, M.; Colombo, R.; Filippa, G.; Julitta, T.; Manca, G.; Siniscalco, C.; Morra di Cella, U.; et al. Phenology and Carbon Dioxide Source/Sink Strength of a Subalpine Grassland in Response to an Exceptionally Short Snow Season. *Environ. Res. Lett.* **2013**, *8*, 025008. [CrossRef]

26. Jin, H.; Jönsson, A.M.; Bolmgren, K.; Langvall, O.; Eklundh, L. Disentangling Remotely-Sensed Plant Phenology and Snow Seasonality at Northern Europe Using MODIS and the Plant Phenology Index. *Remote Sens. Environ.* **2017**, *198*, 203–212. [CrossRef]
27. Jin, H.; Eklundh, L. A Physically Based Vegetation Index for Improved Monitoring of Plant Phenology. *Remote Sens. Environ.* **2014**, *152*, 512–525. [CrossRef]
28. Sparks, T.; Menzel, A. Plant Phenology Changes and Climate Change. In *Encyclopedia of Biodiversity*; Academic Press: New York, NY, USA, 2013; pp. 103–108, ISBN 9780123847201.
29. Core Writing Team; Pachauri, R.K.; Meyer, L.A. (Eds.) *Climate Change 2014: Synthesis Report. Contribution of Working Groups I, II and III to the Fifth Assessment Report of the Intergovernmental Panel on Climate Change*; IPCC: Geneva, Switzerland, 2014.
30. *FAO Statistical Yearbook 2013. World Food and Agriculture*; Food and Agriculture Organization for the United Nations: Rome, Italy, 2013.
31. Ni, J. Carbon Storage in Grasslands of China. *J. Arid Environ.* **2002**, *50*, 205–218. [CrossRef]
32. Ponzetta, M.P.; Cervasio, F.; Crocetti, C.; Messeri, A.; Argenti, G. Habitat Improvements with Wildlife Purposes in a Grazed Area on the Apennine Mountains. *Ital. J. Agron.* **2010**, *5*, 233–238. [CrossRef]
33. Hao, R.; Yu, D.; Liu, Y.; Liu, Y.; Qiao, J.; Wang, X.; Du, J. Impacts of Changes in Climate and Landscape Pattern on Ecosystem Services. *Sci. Total Environ.* **2017**, *579*, 718–728. [CrossRef]
34. Bengtsson, J.; Bullock, J.M.; Egoh, B.; Everson, C.; Everson, T.; O'Connor, T.; O'Farrell, P.J.; Smith, H.G.; Lindborg, R. Grasslands—More Important for Ecosystem Services than You Might Think. *Ecosphere* **2019**, *10*, 1–20. [CrossRef]
35. Dibari, C.; Costafreda-Aumedes, S.; Argenti, G.; Bindi, M.; Carotenuto, F.; Moriondo, M.; Padovan, G.; Pardini, A.; Staglianò, N.; Vagnoli, C.; et al. Expected Changes to Alpine Pastures in Extent and Composition under Future Climate Conditions. *Agronomy* **2020**, *10*, 926. [CrossRef]
36. Menzel, A.; Yuan, Y.; Matiu, M.; Sparks, T.; Scheifinger, H.; Gehrig, R.; Estrella, N. Climate Change Fingerprints in Recent European Plant Phenology. *Glob. Chang. Biol.* **2020**, *26*, 2599–2612. [CrossRef] [PubMed]
37. Gong, Z.; Kawamura, K.; Ishikawa, N.; Goto, M.; Wulan, T.; Alateng, D.; Yin, T.; Ito, Y. MODIS Normalized Difference Vegetation Index (NDVI) and Vegetation Phenology Dynamics in the Inner Mongolia Grassland. *Solid Earth* **2015**, *6*, 1185–1194. [CrossRef]
38. Stöckli, R.; Vidale, P.L. European Plant Phenology and Climate as Seen in a 20-Year AVHRR Land-Surface Parameter Dataset. *Int. J. Remote Sens.* **2004**, *25*, 3303–3330. [CrossRef]
39. Pastorello, G.; Trotta, C.; Canfora, E.; Chu, H.; Christianson, D.; Cheah, Y.W.; Poindexter, C.; Chen, J.; Elbashandy, A.; Humphrey, M.; et al. The FLUXNET2015 Dataset and the ONEFlux Processing Pipeline for Eddy Covariance Data. *Sci. Data* **2020**, *7*, 225. [CrossRef] [PubMed]
40. Estimate of Vegetation Production of Terrestrial Ecosystem. In *Advanced Remote Sensing*, 2nd ed.; Academic Press: New York, NY, USA, 2020; ISBN 9780128158265.
41. Wohlfahrt, G.; Hammerle, A.; Haslwanter, A.; Bahn, M.; Tappeiner, U.; Cernusca, A. Seasonal and Inter-Annual Variability of the Net Ecosystem CO_2 Exchange of a Temperate Mountain Grassland: Effects of Weather and Management. *J. Geophys. Res. Atmos.* **2008**, *113*, 1–14. [CrossRef] [PubMed]
42. Merbold, L.; Eugster, W.; Stieger, J.; Zahniser, M.; Nelson, D.; Buchmann, N. Greenhouse Gas Budget (CO_2, CH_4 and N_2O) of Intensively Managed Grassland Following Restoration. *Glob. Chang. Biol.* **2014**, *20*, 1913–1928. [CrossRef] [PubMed]
43. Imer, D.; Merbold, L.; Eugster, W.; Buchmann, N. Temporal and Spatial Variations of Soil CO_2, CH_4 and N_2O Fluxes at Three Differently Managed Grasslands. *Biogeosciences* **2013**, *10*, 5931–5945. [CrossRef]
44. Prescher, A.K.; Grünwald, T.; Bernhofer, C. Land Use Regulates Carbon Budgets in Eastern Germany: From NEE to NBP. *Agric. For. Meteorol.* **2010**, *150*, 1016–1025. [CrossRef]
45. Post, H.; Franssen, H.J.H.; Graf, A.; Schmidt, M.; Vereecken, H. Uncertainty Analysis of Eddy Covariance CO_2 Flux Measurements for Different EC Tower Distances Using an Extended Two-Tower Approach. *Biogeosciences* **2015**, *12*, 1205–1221. [CrossRef]
46. Marcolla, B.; Cescatti, A.; Manca, G.; Zorer, R.; Cavagna, M.; Fiora, A.; Gianelle, D.; Rodeghiero, M.; Sottocornola, M.; Zampedri, R. Climatic Controls and Ecosystem Responses Drive the Inter-Annual Variability of the Net Ecosystem Exchange of an Alpine Meadow. *Agric. For. Meteorol.* **2011**, *151*, 1233–1243. [CrossRef]
47. Camps-Valls, G.; Campos-Taberner, M.; Moreno-Martínez, Á.; Walther, S.; Duveiller, G.; Cescatti, A.; Mahecha, M.D.; Muñoz-Marí, J.; García-Haro, F.J.; Guanter, L.; et al. A Unified Vegetation Index for Quantifying the Terrestrial Biosphere. *Sci. Adv.* **2021**, *7*, 1–10. [CrossRef] [PubMed]
48. Elmore, A.J.; Guinn, S.M.; Minsley, B.J.; Richardson, A.D. Landscape Controls on the Timing of Spring, Autumn, and Growing Season Length in Mid-Atlantic Forests. *Glob. Chang. Biol.* **2012**, *18*, 656–674. [CrossRef]
49. Gu, L.; Post, W.; Baldocchi, D.D.; Black, T.; Suyker, A.; Verma, S.; Vesala, T.; Wofsy, S. Characterizing the Seasonal Dynamics of Plant Community Photosynthesis across a Range of Vegetation Types. In *Phenology of Ecosystem Processes*; Springer: New York, NY, USA, 2009; pp. 35–58.
50. Beck, P.S.A.; Atzberger, C.; Høgda, K.A.; Johansen, B.; Skidmore, A.K. Improved Monitoring of Vegetation Dynamics at Very High Latitudes: A New Method Using MODIS NDVI. *Remote Sens. Environ.* **2006**, *100*, 321–334. [CrossRef]
51. Klosterman, S.T.; Hufkens, K.; Gray, J.M.; Melaas, E.; Sonnentag, O.; Lavine, I.; Mitchell, L.; Norman, R.; Friedl, M.A.; Richardson, A.D. Evaluating Remote Sensing of Deciduous Forest Phenology at Multiple Spatial Scales Using PhenoCam Imagery. *Biogeosciences* **2014**, *11*, 4305–4320. [CrossRef]
52. Kline, M. *Calculus: An Intuitive and Physical Approach*, 2nd ed.; Dover Publications: Mineola, NY, USA, 1998.

53. Zheng, Z.; Zhu, W. Uncertainty of Remote Sensing Data in Monitoring Vegetation Phenology: A Comparison of MODIS C5 and C6 Vegetation Index Products on the Tibetan Plateau. *Remote Sens.* **2017**, *9*, 1288. [CrossRef]
54. Xu, X.; Zhou, G.; Du, H.; Mao, F.; Xu, L.; Li, X.; Liu, L. Combined MODIS Land Surface Temperature and Greenness Data for Modeling Vegetation Phenology, Physiology, and Gross Primary Production in Terrestrial Ecosystems. *Sci. Total Environ.* **2020**, *726*, 137948. [CrossRef]
55. Ren, S.; Vitasse, Y.; Chen, X.; Peichl, M.; An, S. Assessing the Relative Importance of Sunshine, Temperature, Precipitation, and Spring Phenology in Regulating Leaf Senescence Timing of Herbaceous Species in China. *Agric. For. Meteorol.* **2022**, *313*, 108770. [CrossRef]
56. White, M.A.; de Beurs, K.M.; Didan, K.; Inouye, D.W.; Richardson, A.D.; Jensen, O.P.; O'Keefe, J.; Zhang, G.; Nemani, R.R.; van Leeuwen, W.J.D.; et al. Intercomparison, Interpretation, and Assessment of Spring Phenology in North America Estimated from Remote Sensing for 1982–2006. *Glob. Chang. Biol.* **2009**, *15*, 2335–2359. [CrossRef]
57. Badeck, F.W.; Bondeau, A.; Böttcher, K.; Doktor, D.; Lucht, W.; Schaber, J.; Sitch, S. Responses of Spring Phenology to Climate Change. *New Phytol.* **2004**, *162*, 295–309. [CrossRef]
58. Xu, H.; Twine, T.E.; Yang, X. Evaluating Remotely Sensed Phenological Metrics in a Dynamic Ecosystem Model. *Remote Sens.* **2014**, *6*, 4660–4686. [CrossRef]
59. Wu, C.; Peng, D.; Soudani, K.; Siebicke, L.; Gough, C.M.; Arain, M.A.; Bohrer, G.; Lafleur, P.M.; Peichl, M.; Gonsamo, A.; et al. Land Surface Phenology Derived from Normalized Difference Vegetation Index (NDVI) at Global FLUXNET Sites. *Agric. For. Meteorol.* **2017**, *233*, 171–182. [CrossRef]
60. Gallinat, A.S.; Primack, R.B.; Wagner, D.L. Autumn, the Neglected Season in Climate Change Research. *Trends Ecol. Evol.* **2015**, *30*, 169–176. [CrossRef] [PubMed]
61. Adu, B.; Qin, G.; Li, C.; Wu, J. Grassland Phenology's Sensitivity to Extreme Climate Indices in the Sichuan Province, Western China. *Atmosphere* **2021**, *12*, 1650. [CrossRef]
62. Li, X.; Guo, W.; Li, S.; Zhang, J.; Ni, X. The Different Impacts of the Daytime and Nighttime Land Surface Temperatures on the Alpine Grassland Phenology. *Ecosphere* **2021**, *12*, e03578. [CrossRef]
63. Ren, S.; Li, Y.; Peichl, M. Diverse Effects of Climate at Different Times on Grassland Phenology in Mid-Latitude of the Northern Hemisphere. *Ecol. Indic.* **2020**, *113*, 106260. [CrossRef]
64. Hou, X.; Gao, S.; Niu, Z.; Xu, Z. Extracting Grassland Vegetation Phenology in North China Based on Cumulative SPOT-VEGETATION NDVI Data. *Int. J. Remote Sens.* **2014**, *35*, 3316–3330. [CrossRef]
65. Sadras, V.O.; Monzon, J.P. Modelled Wheat Phenology Captures Rising Temperature Trends: Shortened Time to Flowering and Maturity in Australia and Argentina. *Field Crop. Res.* **2006**, *99*, 136–146. [CrossRef]
66. Sadras, V.O.; Moran, M.A. Agricultural and Forest Meteorology Nonlinear Effects of Elevated Temperature on Grapevine Phenology. *Agric. For. Meteorol.* **2013**, *173*, 107–115. [CrossRef]
67. Cleland, E.E.; Chiariello, N.R.; Loarie, S.R.; Mooney, H.A.; Field, C.B. Diverse Responses of Phenology to Global Changes in a Grassland Ecosystem. *Proc. Natl. Acad. Sci. USA* **2006**, *103*, 13740–13744. [CrossRef]
68. Hua, X.; Sirguey, P.; Ohlemüller, R. Recent Trends in the Timing of the Growing Season in New Zealand's Natural and Semi-Natural Grasslands. *GIScience Remote Sens.* **2021**, *58*, 1090–1111. [CrossRef]
69. Ganjurjav, H.; Gornish, E.S.; Hu, G.; Wan, Y.; Li, Y.; Danjiu, L.; Gao, Q. Temperature Leads to Annual Changes of Plant Community Composition in Alpine Grasslands on the Qinghai-Tibetan Plateau. *Environ. Monit. Assess.* **2018**, *190*, 585. [CrossRef] [PubMed]
70. Vitasse, Y.; Ursenbacher, S.; Klein, G.; Bohnenstengel, T.; Chittaro, Y.; Delestrade, A.; Monnerat, C.; Rebetez, M.; Rixen, C.; Strebel, N.; et al. Phenological and Elevational Shifts of Plants, Animals and Fungi under Climate Change in the European Alps. *Biol. Rev. Camb. Philos. Soc.* **2021**, *41*, 1816–1835. [CrossRef] [PubMed]
71. Hock, R.; Rasul, G.; Adler, C.; Cáceres, B.; Gruber, S.; Hirabayashi, Y.; Jackson, M.; Kääb, A.; Kang, S.; Kutuzov, S.; et al. Chapter 2: High Mountain Areas. In *IPCC Special Report on the Ocean and Cryosphere in a Changing Climate*; Cambridge University Press: Cambridge, UK, 2019; pp. 131–202.
72. Klein, G. Unchanged Risk of Frost Exposure for Subalpine and Alpine Plants after Snowmelt in Switzerland despite Climate Warming. *Int. J. Biometeorol.* **2018**, *62*, 1755–1762. [CrossRef]
73. Körner, C. Life under and in Snow: Protection and Limitation. In *Alpine Plant Life*; Springer: Cham, Switzerland, 2021; ISBN 9783030595371.
74. Vorkauf, M.; Kahmen, A.; Körner, C.; Hiltbrunner, E. Flowering Phenology in Alpine Grassland Strongly Responds to Shifts in Snowmelt but Weakly to Summer Drought. *Alp. Bot.* **2021**, *131*, 73–88. [CrossRef]
75. Grippa, M.; Kergoat, L.; Toan, T.L.; Mognard, N.M.; Delbart, N.; Hermitte, J.L. The Impact of Snow Depth and Snowmelt on the Vegetation Variability over Central Siberia. *Geophys. Res. Lett.* **2005**, *32*, 2–5. [CrossRef]
76. Xie, J.; Hüsler, F.; de Jong, R.; Chimani, B.; Asam, S. Spring Temperature and Snow Cover Climatology Drive the Advanced Springtime Phenology (1991–2014) in the European Alps. *J. Geophys. Res. Biogeosciences* **2021**, *126*, e2020JG006150. [CrossRef]
77. Jerome, D.K.; Petry, W.K.; Mooney, K.A.; Iler, A.M. Snow Melt Timing Acts Independently and in Conjunction with Temperature Accumulation to Drive Subalpine Plant Phenology. *Glob. Chang. Biol.* **2021**, *27*, 5054–5069. [CrossRef]
78. Xu, L.; Zhang, X.; Wang, Y.; Fu, Y.; Yan, H.; Qian, S.; Cheng, L. Drivers of Phenology Shifts and Their Effect on Productivity in Northern Grassland of China during 1984–2017—Evidence from Long-Term Observational Data. *Int. J. Biometeorol.* **2021**, *65*, 527–539. [CrossRef]

79. Weisberg, P.J.; Dilts, T.E.; Greenberg, J.A.; Johnson, K.N.; Pai, H.; Sladek, C.; Kratt, C.; Tyler, S.W.; Ready, A. Phenology-Based Classification of Invasive Annual Grasses to the Species Level. *Remote Sens. Environ.* **2021**, *263*, 112568. [CrossRef]
80. Mutanga, O.; Shoko, C. Monitoring the Spatio-Temporal Variations of C3/C4 Grass Species Using Multispectral Satellite Data. In Proceedings of the 2018 IEEE International Geoscience and Remote Sensing Symposium, Valencia, Spain, 22–27 July 2018; pp. 8988–8991. [CrossRef]
81. Castillioni, K.; Newman, G.S.; Souza, L.; Iler, A.M. Effects of Drought on Grassland Phenology Depend on Functional Types. *New Phytol.* **2022**, *236*, 1558–1571. [CrossRef] [PubMed]
82. Weil, G.; Lensky, I.M.; Levin, N. Using Ground Observations of a Digital Camera in the VIS-NIR Range for Quantifying the Phenology of Mediterranean Woody Species. *Int. J. Appl. Earth Obs. Geoinf.* **2017**, *62*, 88–101. [CrossRef]
83. Dibari, C.; Pulina, A.; Argenti, G.; Aglietti, C.; Bindi, M.; Moriondo, M.; Mula, L.; Pasqui, M.; Seddaiu, G.; Roggero, P.P. Climate Change Impacts on the Alpine, Continental and Mediterranean Grassland Systems of Italy: A Review. *Ital. J. Agron.* **2021**, *16*, 1843. [CrossRef]